# Factorization of the Reconstruction Problem in Circular Cone-Beam Tomography and its Use for Stability Analysis

Frank Dennerlein, *Student Member, IEEE,* Frédéric Noo, *Member, IEEE,* Joachim Hornegger, and Günter Lauritsch

***Abstract*— In this article, we propose a novel factorization of the circular cone-beam (CB) reconstruction problem into a set of independent 2D inversion problems. This factorization is established in the context of modern two-step Hilbert reconstruction methods by combining the ideas of an empirically derived CB inversion approach with a firm and exact theory. We were able to accurately discretize these 2D inversion problems, which allows a detailed investigation of CB reconstruction by using the Singular Value Decomposition and also allows efficient iterative reconstruction approaches. The introduced theory is applied for preliminary studies of the stability of circular CB tomography assuming a short object. We analyzed, how the radius of the circular scan affects the stability and investigated the effect of an additional linear scan onto the condition of the problem. Numerical results are presented for a disc phantom.**

## I. Introduction

Three-dimensional (3D) image reconstruction from cone-beam (CB) data acquired on a circular trajectory is an active subject of research nowadays. This research is motivated by recent advances in detector technology and the fact that the circular trajectory is of all possible data acquisition configurations the easiest one to implement. Unfortunately, CB data on a circle do not provide enough information to achieve accurate reconstruction [1], and this problem becomes more acute when the data is only known over a segment of the circle instead of the full circle, which represents an important practical situation.

Several reconstruction techniques have been developed for reconstruction from CB data acquired along a partial circular trajectory, but no existing technique lies on a firm theoretical ground while allowing some degree of data truncation. In medical imaging, however, CB data are always truncated in at least one direction. The existence of a firm theory supporting the algorithm is important to be able to predict artifacts and devise iterative corrections reducing these artifacts.

In 2005, Yu *et al.* [2] proposed a new original method to do reconstructions from circular CB data. This method is a Feldkamp-like extension of the two-step Hilbert method they and others developed for fan-beam tomography [3], [4]. As such, it presents attractive properties: it is efficient, allows axial truncation, allows partial transverse truncation for specific regions-of-interest and does not require data over 360 degrees. However, this method was defined heuristically.

Using the general, exact CB reconstruction theory in [5], we have realized that the basic idea of Yu *et al.* [2] may be used to factorize the CB reconstruction problem into a set of independent 2D inversion problems. Unlike the harmonic decomposition [6], this factorization applies to data on a full-scan as well as to the data on a short-scan. We report below on this factorization and some preliminary use of it to investigate the incompleteness of partial circular CB data.

F. Dennerlein and F. Noo are with the Department of Radiology, University of Utah, Salt Lake City, Utah, USA

E-mail: fdenner@ucair.med.utah.edu

J. Hornegger is with the Institute of Pattern Recognition, University of Erlangen-Nuremberg, Erlangen, Germany

G. Lauritsch is with Siemens AG, Medical Solutions, Forchheim, Germany.

This work was partially supported by a grant of Siemens AG, Medical Solutions and by the U.S. National Institutes of Health (NIH) under grant R01 EB000627. Its contents are solely the responsibilitiy of the authors and do not necessarily represent the official views of the NIH.

## II. Geometry and Data Description

We assume CB data acquisition where the focus of the X-ray source follows a circular trajectory of radius $R$ around the object under investigation. This trajectory may be parametrized by $\lambda$ such that coordinates of the source are obtained as

$$\underline{a}(\lambda) = [R\,\cos\lambda, R\,\sin\lambda, 0]. \tag{1}$$

Let $[0, \lambda_m]$ be the angular range covered in $\lambda$ during the acquisition process. For a full-scan, $\lambda_m = 2\pi$, but here we assume CB data for less than a full-scan trajectory and consequently $\lambda_m < 2\pi$. The function $f(\underline{x})$ with $\underline{x} \in I\!R^3$ represents the distribution of the object X-ray linear attenuation coefficient within the region of interest (ROI). CB data acquisition yields integrals of $f$ along half-lines that start from the source and are each defined by a unit direction vector $\underline{\alpha}$, i.e., we obtain samples of the data function

$$g(\lambda, \underline{\alpha}) = \int_0^\infty dt\, f(\underline{a}(\lambda) + t\underline{\alpha}). \tag{2}$$

## III. Reconstruction Theory

Let us first define a family of planes that intersect the object ROI and are orthogonal to the plane of the source trajectory. There is not much restriction on the definition of this family; the planes may be nicely ordered in space (e.g., parallel to each other) or not. Our preferred configuration is one in which the planes share a common line that is orthogonal to the plane of the circular scan, say the line through the source position at $\lambda = 0$. Planes from this family may be parameterized by an angle $\phi$. Let $\lambda_1(\phi)$ and $\lambda_2(\phi)$ be the parameters,

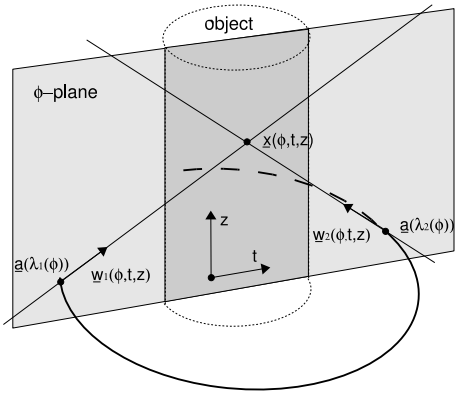


Fig. 1. Illustration of an arbitrary $\phi$-plane. It intersects with the source trajectory at parameters $\lambda_1(\phi)$ and $\lambda_2(\phi)$ and contains the point $\underline{x}$ at which reconstruction is to be achieved. The intermediate function $b$ at $\underline{x}$ is related to the values of the object density $f$ along two lines. Both of them are located in the $\phi$-plane, contain $\underline{x}$ and follow the direction $\underline{w}_1$ and $\underline{w}_2$, respectively.

where the plane of angle $\phi$ (the $\phi$-plane) intersects with the source trajectory. Following our convention, $\lambda_1(\phi) = 0$. In the following, we demonstrate how the circular CB reconstruction problem can be factorized into a set of independent 2D inversion problems, each of which corresponds to finding the density function $f$ on one $\phi$-plane.

For every $\phi$-plane, two Cartesian coordinates $t$ and $z$ can be introduced, with $z$ in the direction orthogonal to the plane of the circular scan. A point within the 3D ROI may then be parametrized using the non-Cartesian coordinates $\underline{x}(\phi, t, z)$.

To reconstruct the object density function $f$ we first differentiate CB data with respect to the curve parameter $\lambda$, while fixing the ray direction $\underline{\alpha}$ to obtain

$$g'(\lambda, \underline{\alpha}) = \lim_{\epsilon \to 0} \frac{g(\lambda + \epsilon, \underline{\alpha}) - g(\lambda - \epsilon, \underline{\alpha})}{2\epsilon}. \tag{3}$$

The differentiated data of (3) is then backprojected onto points of the ROI aligned on a grid which is defined by discretized values of $\phi$, $t$ and $z$. For points of coordinate $\phi$, we backproject only data that is within the interval $\lambda_1(\phi)$ and $\lambda_2(\phi)$. This yields the intermediate function

$$b(\phi, t, z) = \int_{\lambda_1(\phi)}^{\lambda_2(\phi)} \frac{d\lambda}{\|\underline{x}(\phi, t, z) - \underline{a}(\lambda)\|} g'(\lambda, \underline{\alpha}^*(\lambda, \phi, t, z)). \tag{4}$$

In this formula, $\underline{\alpha}^*(\lambda, \phi, t, z)$ denotes the unit vector along the line that connects $\underline{a}(\lambda)$ with $\underline{x}(\phi, t, z)$ during backprojection. The relation between the intermediate result $b$ and the sought function $f$ is given by the following equation [5]:

$$\begin{aligned} \frac{1}{\pi} b(\phi, t, z) &= \int_{-\infty}^{+\infty} \frac{d\tau}{\pi\tau} f\left(\underline{x}(\phi, t, z) + \tau \underline{w}_1(\phi, t, z)\right) \\ &- \int_{-\infty}^{+\infty} \frac{d\tau}{\pi\tau} f\left(\underline{x}(\phi, t, z) + \tau \underline{w}_2(\phi, t, z)\right) \end{aligned} \tag{5}$$

Here, $\underline{w}_1(\phi, t, z)$ (resp. $\underline{w}_2(\phi, t, z)$) is the unit vector from the source position at $\lambda_1(\phi)$ (resp. $\lambda_2(\phi)$) to $\underline{x}(\phi, t, z)$ and both vectors, $\underline{w}_1$ and $\underline{w}_2$, are located in the $\phi$-plane. See Fig. 1 for an illustration.

Hence, for each $\phi$, the quantity $b(\phi, t, z)$, which is directly computable from the CB data is dependent only on the values of $f$ within the plane of angle $\phi$. Finding a solution $f(\phi, t, z)$ to (5) from $b(\phi, t, z)$ at fixed $\phi$ then corresponds to a 2D inversion problem. Circular CB reconstruction is thus factorized through the computation of $b(\phi, t, z)$ into a family of 2D problems, and this factorization applies to any $\phi$-plane such that $\lambda_2(\phi) < \lambda_m$.

## IV. Discretization

The 2D inversion problem for each $\phi$-plane can be discretized into a linear system of equations. Then, a detailed singular value decomposition (SVD) analysis of the stability of the CB reconstruction problem becomes possible. A discretization of (5) is obtained as

$$\underline{b} = \pi(M - N)\underline{f}. \tag{6}$$

Here, the vectors $\underline{f}$ and $\underline{b}$ define samples of the functions $f$ and $b$ in the considered $\phi$-plane and the matrices $M$ and $N$ model the required filtering operations. $M$ represents the first integral on the r.h.s of (5), whereas $N$ represents the second integral. Consider now just one arbitrary sample in $\underline{b}$, corresponding to the point $\underline{x}$ of the ROI. According to (6), it is related to $\underline{f}$ via a certain row of $M$ and $N$, respectively, and we now briefly explain how we found the corresponding matrix elements. The row of $M$ (denoted as $\underline{r}$) can be obtained with the following steps:

a) Determine the filtering line through $\underline{a}(\lambda_1)$ and $\underline{x}$, i.e., compute the vector $\underline{w}_1(\phi, t, z)$.
b) Introduce a sampling on that filtering line by discretizing $\tau$. In general, this sampling does not coincide with the sampling grid of $f$ or $b$.
c) For each filtering line sampling point $P$, determine elements of $\underline{f}$ and linear interpolation coefficients that yield an interpolated value of $f$ at $P$.
d) Approximate the integration in (5) with a weighted sum of the values of $f$ at points $P$. For each $P$, find the corresponding weight that depends on $\tau$.
e) Compose $\underline{r}$ by setting appropriate elements to the product of the interpolation coefficients from c) and the weights from d).

By repeating steps a) to e) from above for all samples of $\underline{b}$, we completely determine the matrix $M$ in a row-by-row strategy. The elements in $N$ are found in an analog manner. Thus, the initial linear system (6) is obtained as desired and reconstruction on the given plane is equivalent to solving (6) for $\underline{f}$.

The system can beneficially incorporate additional knowledge, such as the values of $f$ along the lines of direction $\underline{w}_1$ and $\underline{w}_2$ through $\underline{x}(\phi, t, z)$; these values are within the $\phi$-plane and are part of the measured CB data. Doing so, we obtain an extended system of equations

$$A\underline{f} = \begin{bmatrix} \underline{b} \\ \underline{c} \end{bmatrix}, \tag{7}$$

with $\underline{c}$ denoting elements of the known CB data function that correspond to the additional information. The matrix $A$ is based on $M$ and $N$ from (6) and extended by several rows modeling the additional line integrals. The structure of an exemplary $A$ is presented in Fig. 4.

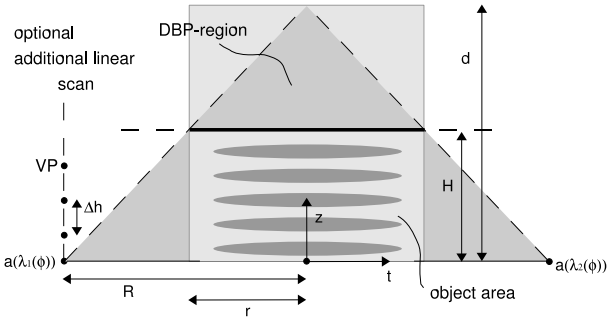


Fig. 2. The $\phi_0$-plane in the evaluated short object scenario (see text). Ray integrals that diverge from vertex points (VPs) located on an additional linear scan segment may be added to the system of equations. By that, we can study the effect of additional data onto the stability of the reconstruction problem.

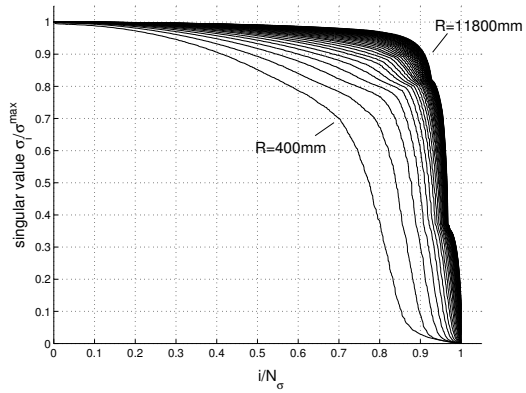


Fig. 3. Normalized singular value spectra $\sigma_i/\max(\sigma_i)$ for various scan radii $R \in [400, 11800]$ mm. The order of the spectra is such that for increasing $R$, the curves enclose a larger area with the coordinate axes.

## V. Experimental Set-Up

For numerical evaluations, we picture circular data acquisition with a virtual detector located at the iso-center. The detector has height $d$ and is vertically positioned such that its lower edge starts at the plane of the circle scan. For our first studies, we further assume that the detector is wide enough so that acquired CB data for $\lambda \in [0, \lambda_m]$ is not truncated in transaxial direction. From $d$ and the scan radius $R$, a *DBP-region* can be geometrically determined, in which the function $b$ is computable from the acquired CB data. For a full-scan, the top boundary of the DBP-region would be cone-shaped. In case of a short scan, however, the symmetry is lost and the shape of the DBP-region gets more complex. We assume now, that the investigated short object fits entirely in a cylinder of radius $r$ and height $H$, which sits on the plane of the circle scan and is centered around the rotational axis of the scan path (the $x_3$-axis). The height $H$ of the object cylinder is set to the maximum value that still ensures that the object does not go beyond the DBP-region.

Using the described set-up, only the reconstruction of $f$ inside and above the plane of the source trajectory can be analyzed. Because of symmetry, however, the obtained result may also be used to deduce the stability for reconstruction of $f$ in regions below that plane.

By applying the suggested factorization theory, the 2D inversion problem for an arbitrary $\phi$-plane can be formulated. Without restriction of generality, we consider the plane that contains $x_3$ and has parameter $\phi_0$ for further analysis, but any other plane would be suitable, too. Fig. 2 illustrates the cross-section of the acquisition geometry with the selected $\phi_0$-plane, presenting a triangular shaped DBP-region with a tightly fitted rectangular bounded object area. These regions are obviously of different size. Hence, a discretization of the functions $f$ and $b$ using an identical sampling pattern and spacing yields vectors $\underline{f}$ and $\underline{b}$ that are not of the same dimension. Following Sec. IV we can determine the linear system of equations, i.e., the matrix $A$, for the $\phi_0$-plane. In the considered set-up, this system is overdetermined.

The matrix $A$ is used to analyze the stability of several geometric variations of the CB reconstruction problem. Investigations are based on (i) the analysis of the singular value spectrum $\sigma_i$ of $A$ and on (ii) the reconstruction from (non-consistent) noisy data $\underline{b}^n$ as $\underline{f}^r = A_\alpha^+ \underline{b}^n$. The pseudo-inverse $A_\alpha^+$ is computed via the SVD and Tikhonov regularization, which relates the singular values $\hat{\sigma}_i$ of $A_\alpha^+$ to the singular values of $A$ as $\hat{\sigma}_i = \sigma_i/(\sigma_i^2 + \alpha^2)$.

## VI. Investigations on the Stability of CB Reconstruction

### A. Effect of the Scan Radius on Circular Cone-Beam CT

In a first experiment, the effect of the scan radius $R$ onto the stability of circular CB reconstruction is studied. We define $d = 25$ cm, $r = 15$ cm and use a Cartesian sampling of the $\phi_0$-plane with $\Delta t = \Delta z = 5$ mm. The radius $R$, however, varies from experiment to experiment by a constant increment of $\Delta R = 300$ mm and covers the interval $R \in [400, 11800]$ mm. The parameter $H$ increases with $R$, so that

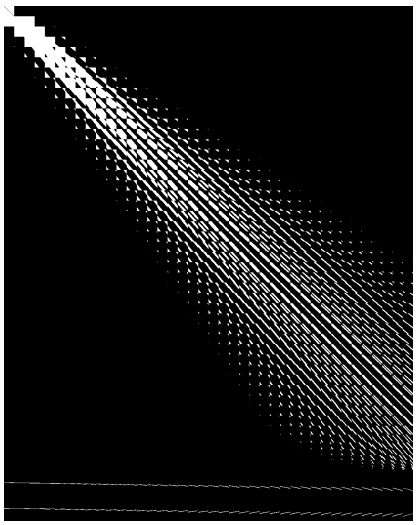

Fig. 4. The non-zero entries (white) of the matrix $A$ for the geometry of Sec. VI-A and $R = 700$ mm. The bottom rows of distinct structure correspond to the additional line integral information, whereas the major part of the $A$ represents the relation given in (5).

the actual dimension of the system matrix $A$ may also vary with $R$. The singular value spectra of $A$ for each radius $R$ are

shown in Fig. 3. Fig. 4 presents the structure of $A$ as obtained for $R = 700$ mm. A selection of singular images of $A$ is given in Fig. 7.

### *B. Effect of an Additional Scan Segment on the Stability*

We now investigate, to what degree the knowledge of additional ray integrals improves the stability of the reconstruction problem. Experiments are performed for a circular scan with $R = 700$ mm, but we also consider additional rays through the object that diverge from a set of vertex points (VPs) and assume that the integrals of $f$ along these rays are known. These VPs are located somewhere on a vertical line that intersects the circle segment at $\lambda = 0$. Since the additional line segment is contained on each $\phi$-plane within the family of planes defined in Sec. III, the 2D inversion problem for each plane may benefit from the additional information. We accurately discretize the line integral information and add it to the linear system of equations for the considered $\phi_0$-plane. Doing so, we obtain an extended matrix - denoted as $A_e$ - which may be analyzed as suggested before.

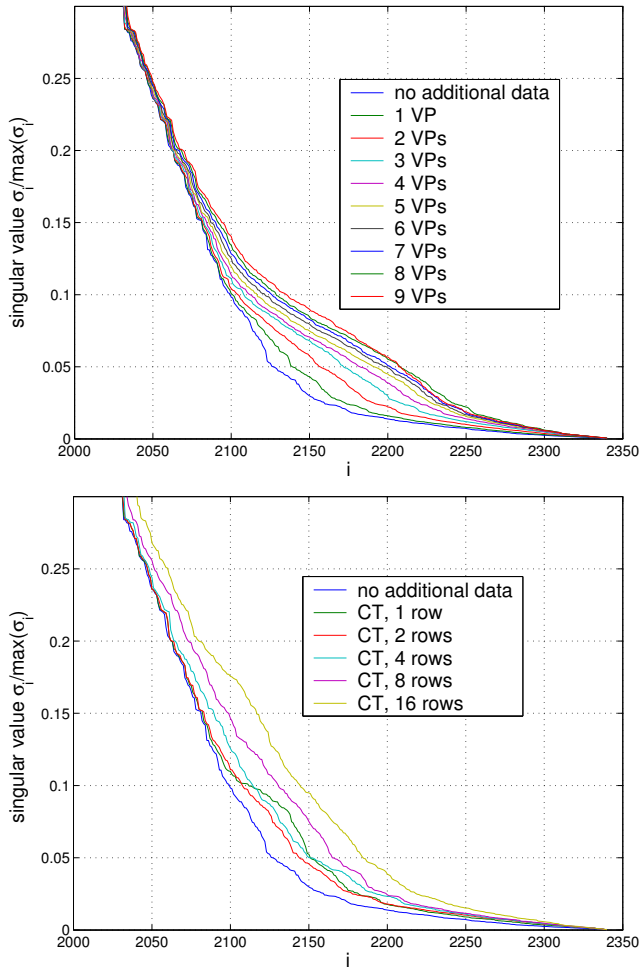


Fig. 5. Singular value spectra of $A_e$ for (top) a few additional VPs and a large fan of rays per VP (C-arm scenario) and (bottom) many additional VPs with only few rays per VP (CT-like scenario). Only the tail region of $\sigma_i$ is presented to illustrate the main deviation between the spectra (colors in the electronic version). The order of the spectra in either case is such that adding more ray integrals to $A_e$ yields an increase of the values of $\sigma_i$.

First, the linear scan is finely sampled, so that many additional VPs are introduced. These VPs are aligned evenly in the interval $[0, H]$ along the line, so that two adjacent VPs differ by $\Delta h = 5$ mm (Fig. 2). For each VP and $\phi$-plane, only

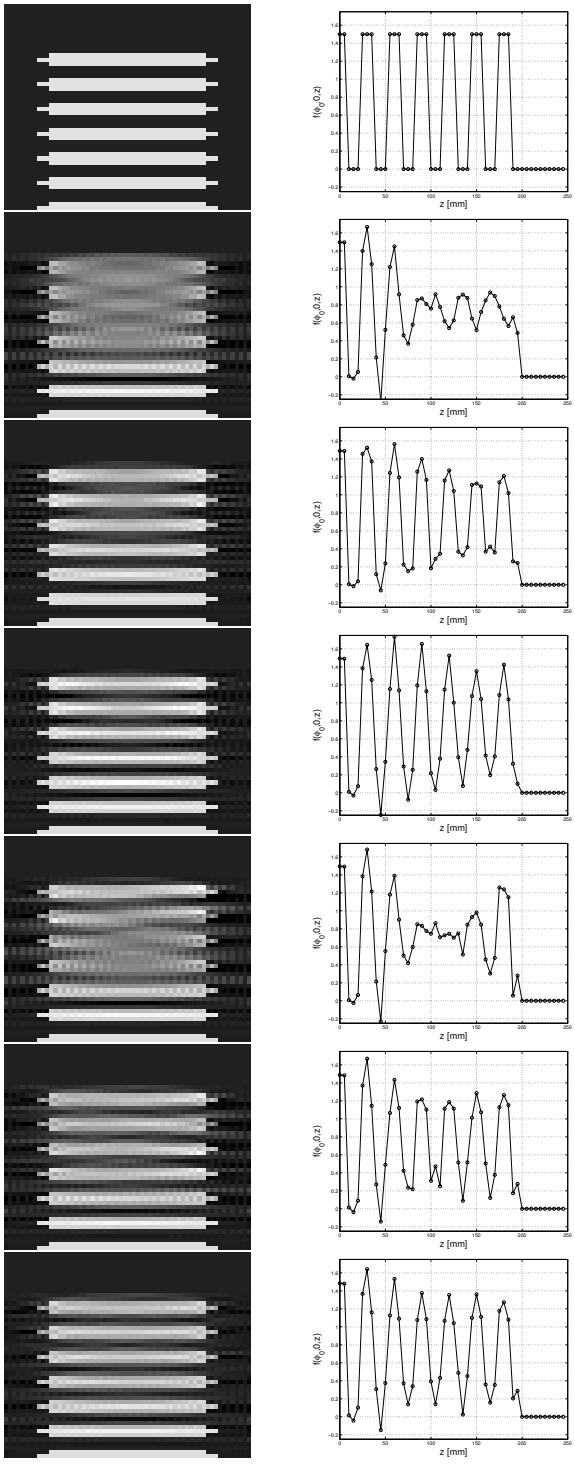


Fig. 6. Reconstructions of a disc phantom from noisy data $\underline{b}^n$. (left) Mean image of $\underline{f}^r$ after 100 noise realizations in a grayscale window $[-.25, 1.75]$, (right) profile of the mean image along the central column ($t = 0$) for $z \in [0, 250]$ mm. From (top) to (bottom): original phantom, no additional VPs, CT-like data for 1 row, CT-like data for 2 rows, C-arm data for 1 additional VP (AVP), for 2 AVPs and for 3 AVPs. Further additional data did not yield a significant visual improvement of the reconstructions.

a few additional rays (1, 2, 4, 8 or 16) are added. Considering the entities on one $\phi$-plane, the rays diverging from each VPs form a fan that is symmetric with respect to horizontal line through the VP. The slopes of two adjacent rays within a fan differ by approximately $7.1 \cdot 10^{-3}$.

In a second experimental series, just a few VPs (2 up to 10) are added on the line scan, again equidistantly covering the interval $[0, H]$. Now, however, we consider 150 rays for each VP and $\phi$-plane, so that for a given $\phi$-plane, the rays diverging from a certain VP compose a large fan. Each fan is again symmetric with respect to the horizontal line through the corresponding VP and the slopes of two consecutive rays differ again by $7.1 \cdot 10^{-3}$.

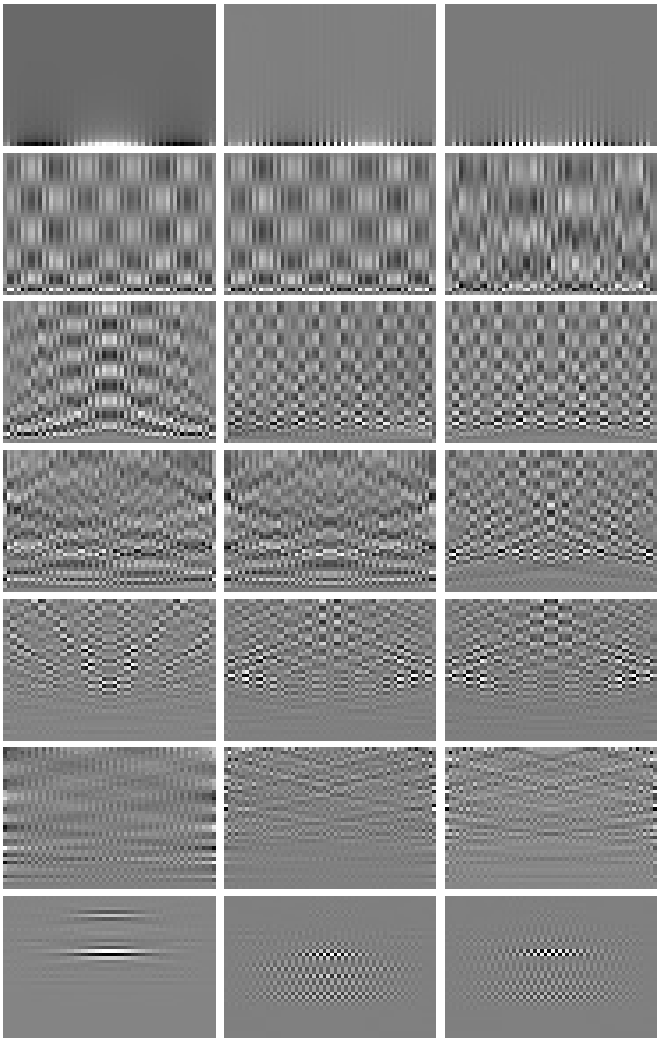

Fig. 7. Singular images of the system matrix $A$ for the acquisition geometry from Sec. VI-A and $R = 700$ mm. In each row, the singular images corresponding to three consecutive singular values $\sigma_i$, $\sigma_{i+1}$ and $\sigma_{i+2}$ are presented. (top to bottom) $i = 1$, $i = 401$, $i = 801$, $i = 1201$, $i = 1601$, $i = 2001$ and $i = 2398$.

Returning to the context of CB tomography, we can find a certain correspondence of these additional ray integrals in the data acquisition process. The consideration of many VPs may be useful to represent CB data acquisition in a multi-slice CT scenario (with 1, 2, 4, 8 or 16 rows). The case of a few, but large sets of diverging rays finds its equivalent in C-arm acquisition. In either case, we expect beneficial effects of the additional data on the stability of CB reconstruction. These effects should be noticeable when analyzing and comparing the properties of the matrices $A_e$ and $A$. Fig. 5 presents the tail of the singular value spectra of $A_e$ corresponding to each of the described scenarios. We also performed reconstructions from noisy data $\underline{b}^n$ of a disc phantom. The level of additive Gaussian noise in $\underline{b}^n$ corresponds to a Gaussian noise in the object with standard deviation of 5 HU. The pseudo-inverse of $A_e$ is obtained by Tikhonov regularization with $\alpha$ set to the 200th singular value, counted from the smallest one backwards. Image results are presented in Fig. 6. As expected, the reconstructions that consider only the circular scan inherit CB artifacts throughout the image and have acceptable quality only for the lower 3 discs. The artifact level for this object is reduced significantly when adding the additional line scan.

## VII. Conclusions

Using the CB reconstruction theory from [5], we set up the main idea of the reconstruction method in [2] into a strong theoretical background, which comes with a factorization of the reconstruction problem. This factorization allows 3D CB reconstruction via solving 2D problems on a set of $\phi$-planes. We were able to accurately discretize the 2D problems, so that a detailed SVD analysis of the reconstruction problem becomes feasible. We performed preliminary studies of the effects of additional scan segments on the stability. The obtained results are consistent with data sufficient conditions, that were established e.g. in the context of the 3D Radon transform [1]. We also notice that adding only a small amount of additional data seems to be sufficient to reduce the artifact level to a high degree. From the introduced factorization theory, efficient 2D iterative CB reconstruction approaches can be developed. These approaches can be able to beneficially incorporate redundant CB data, and can allow reconstruction from partially transaxially truncated CB data.

## References


[1] H. K. Tuy, "An inversion formula for cone beam reconstruction," *SIAM J. Appl. Math.*, vol. 43(3), pp. 546–552, 1983.

[2] L. Yu, D. Xia, Y. Zou, X. Pan, C. A. Pelizzari, and P. Munro, "Image reconstruction from truncated data in circular cone-beam CT and its applications to radiotherapy," in *The 8th intern. meeting on fully 3D image reconstruction in radiology and nuclear medicine*, 2005, pp. 391–395.

[3] X. Pan, Y. Zou, and D. Xia, "Image reconstruction in peripheral and central regions-of-interest and data redundancy," *Med. Phys. 32*, pp. 673–684, 2005.

[4] F. Noo, R. Clackdoyle, and J. D. Pack, "A two-step hilbert transform method for 2d image reconstruction," *Phys. Med. Biol. 49*, pp. 3903–3923, 2004.

[5] J. D. Pack, F. Noo, and R. Clackdoyle, "Cone-beam reconstruction using the backprojection of locally filtered projections," in *IEEE Trans. Med. Imag. 24(1)*, 2005, pp. 70–85.

[6] F. Natterer, *The mathematics of computerized tomography*. Society for Industrial and Applied Mathematics Philadelphia, PA, USA, 2001.